Tribology Letters (2024) 72:106
https://doi.org/10.1007/s11249-024-01905-w

ORIGINAL PAPER

Competition Between Growth and Removal in Zirconia Nanocrystal-Derived Tribofilms: The Role of Co-additives

Parker LaMascus[1] · Meagan B. Elinski[1,2] · Daniel Delghandi[1,3] · Pranjal Nautiyal[1,4] · Julia Griffin[5] · Lei Zheng[6] · Andrew Jackson[1,6] · Robert J. Wiacek[6] · Robert W. Carpick[1]

Received: 25 June 2024 / Accepted: 5 August 2024

Abstract

Antiwear additives permit energy-efficient lubrication of gearboxes, bearings, and other tribological interfaces. We study zirconia (ZrO_2) nanocrystal additives, which readily form protective tribofilms in tribological contacts. Our prior work demonstrated cooperative antiwear performance between ZrO_2 and the S- and P-based co-additives in fully formulated hydrocarbon gear oils. Here, we extend that work by examining the growth kinetics of the ZrO_2 tribofilms, including the influence of the co-additives. In the boundary lubrication regime for mixed rolling-sliding contacts, the initial phase of ZrO_2 tribofilm growth is soon overtaken by removal processes, phenomena whose importance has gone unnoticed in prior work. Tribofilm removal affects the steady-state thickness and morphology of the tribofilm as well as its growth kinetics. The S- and P-based co-additives are incorporated into the ZrO_2 tribofilm, and alter the competition between the growth and removal processes, increasing initial net growth rates per contact cycle and contributing to a more polished final interface. This work highlights the significance of removal processes in determining tribofilm antiwear performance, and suggests several routes for improving tribofilm growth kinetics using co-additives.

Graphical abstract

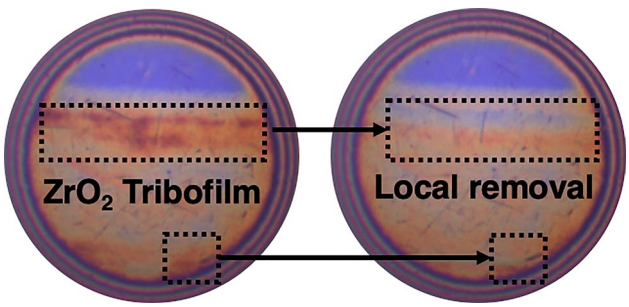

Keywords Nanoparticles · Nanocrystals · Tribofilms · Extreme pressure additives · Tribosintering · Low viscosity gear oil · Coadditives · Elastohydrodynamic lubrication

✉ Robert W. Carpick
carpick@seas.upenn.edu

[1] Department of Mechanical Engineering & Applied Mechanics, University of Pennsylvania, Philadelphia, PA 19104, USA

[2] Present Address: Department of Chemistry, Hope College, Holland, MI 49423, USA

[3] Present Address: Department of Mechanical Engineering, Stanford University, Stanford, CA 94305, USA

[4] Present Address: Department of Mechanical and Aerospace Engineering, Oklahoma State University, Stillwater, OK, USA

[5] Department of Chemistry, Mount Holyoke College, South Hadley, MA 01075, USA

[6] Pixelligent Technologies LLC, Baltimore, MD 21224, USA

Published online: 21 August 2024

1 Introduction

Industrial and commercial machines rely on lubricants to reduce friction and wear of contacting components [1]. Low-viscosity lubricants can decrease churning losses in such machines, significantly reducing energy and revenue costs [2]. However, contacts lubricated with lower-viscosity lubricants are more likely to enter mixed and boundary lubrication regimes [1, 3]. To reduce wear from surface contact, low-viscosity lubricant blends typically include antiwear (AW) additives, such as zinc dialkyldithiophosphates (ZDDPs) [4–6] or metal oxide nanoparticles [7–10], or other additive classes like sulfur- or phosphorus-based extreme pressure (EP) additives [11].

Zirconium dioxide (ZrO_2) NCs are an appealing candidate as next-generation AW additives since they are free from sulfate ash to comply with new environmental regulations [12–14]. The potential of several metal oxide NCs as AW additives was demonstrated by Kato and Komai [10], who used a pin-on-disc tribometer and dry nanopowders to form tribofilms from nine different metal oxide species. Though a dry contact in pure sliding does not emulate liquid-lubricated gearbox or bearing conditions, Kato and Komai [10] nonetheless showed that oxide species with higher oxygen diffusivity prevented wear more effectively, which they attributed to faster tribofilm formation through a stress-assisted sintering mechanism named "tribosintering" by Adachi and Kato [15]. Subsequently, researchers showed that the nanoparticles suspended in liquid lubricants can form tribofilms via tribosintering when subjected to tribological sliding in macroscale tribotests [16, 17]. Other studies of metal oxide nanoparticle additives claim other mechanisms, such as surface healing, polishing, or a ball-bearing action that converts sliding friction to rolling friction [18, 19].

To study AW tribofilm formation with greater verisimilitude, later work employed the atomic force microscopy (AFM) technique of Gosvami et al. [5], which provides lubricated single-asperity contacts in the boundary regime under pure sliding and permits concurrent measurement of tribofilm thickness and morphology. However, AFM has so far been limited to low sliding speeds (at most a few hundred μm/s). Khare et al. [20] used this technique to show that ZrO_2 AW tribofilms derived from ZrO_2 NCs in polyalphaolefin (PAO) base oil form in three distinct stages: a nucleation or induction period with limited growth, followed by a linear growth regime, and ending in thickness saturation. Khare et al. [20] expanded on the tribosintering mechanism of Kato and Komai for ZrO_2 tribofilm formation by showing that nanoscale ZrO_2 tribofilms grow from NC suspensions in lubricant, and that tribofilm growth rates are pressure dependent but relatively independent of temperature (unlike the Arrhenius growth kinetics of ZDDPs, e.g., [20, 21]).

Tribosintering, a process by which heat and stress drive the nanoparticles to form a dense, surface-bound solid phase, is not well understood [20]. Experiments by Hernández Battez et al. created antiwear tribofilms from metal oxide nanoparticle additives, achieving more realistic loads and steel substrates, but limited by pure sliding conditions [16, 17]. Work by Thrush et al. [22–24] and Elinski et al. [8] on ZrO_2 NCs appealed to the tribosintering mechanism to explain their results in the Mini-Traction Machine (MTM) which achieved mixed rolling and sliding conditions. Elinski et al. showed that scuffing damage seen for MTM experiments in pure PAO is prevented for the same PAO with 1 wt.% ZrO_2 NCs added, attributed to the presence of a protective tribofilm formed via tribosintering [8]. The set of studies by Thrush et al., respectively, demonstrated that higher NC concentrations [22], contact pressures [23], and temperatures [24] benefit tribofilm growth rate for MTM experiments conducted with polyalphaolefin (PAO) base oils and the same ZrO_2 NCs. Lahouij et al. also observed ZrO_2 tribofilm formation via tribosintering for the same NCs in PAO in harsh micropitting rig (MPR) tests, where the steel surfaces are much rougher and the primary failure mode is pitting rather than the MTM's scuffing [25].

Benefits of ZrO_2 tribofilms formed via tribosintering are also seen in lubricants with other AW/EP co-additives present. Elinski et al. [8] test ZrO_2 NC additives in an especially relevant lubricant, 75W-80, which has the same S- and P-based AW/EP additive package as the commercial 75W-90, but a reduced viscosity that yields energy efficiency at the cost of surface separation. They observe that ZrO_2 tribofilms formed with S-/P-based co-additives evince less substrate wear, which they attribute to the fast-acting anti-scuffing co-additives preventing initial damage while the thicker ZrO_2 AW tribofilm nucleates [8]. They also hypothesize that the co-additives lead to faster tribosintering of the ZrO_2 NCs [8]. Consistent with this, Demas et al. [26] observe in MPR tests that ZrO_2 NCs in the same fully formulated 75W-80 gear oil used by Elinski et al.[8] prevent scuffing under conditions where NC-free gear oil scuffs. Collectively, these studies demonstrate significant potential for ZrO_2 NCs to function effectively as AW additives. Though all these studies employ more application-relevant contact conditions than AFM, the lack of connection to nanoscale phenomena and observation hampers understanding. Maximizing NC AW performance and translating that to practice necessitates greater mechanistic understanding of tribofilm growth.

We employ a mini-traction machine (MTM) and polyalphaolefin (PAO)-lubricated bearing steel to study the AW performance of ZrO_2 NCs. We vary the slide-to-roll ratio (SRR) between steel ball and disc specimens to replicate

a variety of application-relevant contact conditions, from the teeth of a gear at higher SRR to the rollers of a bearing at lower SRR. Using a novel analysis method, we obtain tribofilm thickness data with high temporal resolution, and use this to demonstrate nanoscale tribofilm removal which occurs alongside tribosintering-driven growth. When commercial S- and P-based AW/EP co-additives are included in the PAO, the ZrO_2 tribofilms form more rapidly, validating the hypothesis of Elinski et al. [8]. Moreover, our insight into the removal process demonstrates that co-additives can benefit tribofilm performance by leading to a smoother interface at steady state.

2 Experimental Methods

2.1 Mini-Traction Machine and Spacer Layer Imaging Method

We use precisely the method described by Elinski et al. [8]; for full details, see Sects. 2.1–2.3 of that work, with a slight modification to our solvents used for post-processing, as described in the erratum to that work [27]. The main instrument for this method is the Mini-Traction Machine (MTM, PCS Instruments, London, UK), a ball-on-disc tribometer which permits lubricated tribological testing and in situ measurements of rolling and/or sliding speeds, and traction. The Spacer Layer Imaging Method (SLIM) that accompanies the MTM measures tribofilm thickness at a single location on the MTM ball specimen [28]. Experimental parameters are given in Table 1.

Table 1 Summary of MTM Testing Conditions

MTM entrainment speed	150 mm/s
Slide-Roll Ratio (SRR)	Independent variable: 25%, 50%, and 100%
Temperature	100 °C
Test duration	2 h (62,000–110,000 contact cycles on the ball, depending on SRR)
Applied load	50 N (1.11 GPa maximum Hertzian pressure)

The figures in this work will typically have a normalized x-axis of Ball Contact Cycles. The equation used for normalization is $n_{ball} = t \bullet v_{ball}/r_{ball}$, where t is the seconds recorded by the MTM, v_{ball} is the ball speed recorded by the MTM, and ball radius r_{ball} is assumed a constant 8.673 mm.

Table 2 contains information on the materials used in the MTM. The steel tribopair and fluid blends were selected to mimic conditions in high-performance gears or bearings. Polyalphaolefin (PAO) is a common base stock, and 75W-80 is a lower-viscosity version of the commercial oil 75W-90. The latter blends contain proprietary S- and P-based co-additives for AW and EP protection.

The materials of Table 2 were carefully chosen to enforce a single independent variable, the presence of co-additives. The elastohydrodynamic (EHD) characteristics of the base oils are nearly identical, and ZrO_2 dispersed in either oil at 1wt% did not significantly affect the viscosity [22]. The only significant difference between PAO10 and 75W-80 is the presence of the commercial S- and P-based AW and EP co-additives in the latter.

2.2 White Light Interferometry

White light interferometry (WLI) measures tribofilm roughness. We used a Zygo NewView interferometer, sputter-coating our MTM specimens with ~ 25 nm Au–Pd to enhance the uniformity of light reflection [29]. RMS roughness is calculated on a 300 µm × 500 µm area. Notably, this WLI data are only taken at the end of each traction test, as the Au–Pd coating process would disrupt the tribology of the interface, meaning that the number of contact cycles on each end-of-test ball specimen is not constant. Therefore, WLI is mostly used to contextualize our SLIM results qualitatively. Namely, if the WLI's measurement of the tribofilm's height above the adjacent substrate to be smaller in magnitude than the SLIM's measurement of the transparent tribofilm's total thickness, it implies that the tribofilm is embedded into the steel substrate through plasticity or wear prior to tribofilm growth [8].

Table 2 Summary of Specimen Properties

Specimens	MTM: 52,100 Steel (< 20 nm RMS roughness, ball radius 8.673 mm)
Base Oil and Viscosity at 100 °C	PAO10: 10 cSt 75W-80: 9.6 cSt
Film Thickness parameter, λ	PAO10 + 1wt% ZrO_2: 2.03 75W-80 + 1wt% ZrO_2: 1.98
Nanocrystals	ZrO_2 nanocrystals: 5-nm diameter, capped with organic ligand for solubility (PixClear PC14-10-L01), cubic phase, 1 wt% dispersion in both oils

2.3 Time-of-flight Secondary Ion Mass Spectrometry

Time-of-flight secondary ion mass spectrometry (ToF-SIMS) measures spatially resolved chemical composition of tribofilms deposited on MTM disc specimens at the end of test. A TOFWERK CTOF ToF-SIMS spectrometer (TOFWERK, Thun, Switzerland) installed inside a Tescan S852X FIB-SEM system (Tescan, Brno, Czech Republic) was employed. A Xe^+ ion beam (30 kV voltage, 30 nA current, and 10 µs dwell time) was used to sputter the tribofilm and the surrounding region to determine chemical composition as a function of tribofilm thickness. To establish a conversion from frames to nm, WLI is used before and after milling to measure the depth of the milled trench.

3 Results and Discussion

3.1 Non-monotonic Tribofilm Growth

For all the contact conditions and blends under consideration, we observe the formation of thick, surface-bound tribofilms (Fig. 1, bottom). As mentioned above, Elinski et al. [8], using identical blends and experimental conditions to this study, show that these tribofilms prevent scuffing and alleviate wear of the substrate, offering substantial practical benefit. We also observe that a higher SRR hastens the onset of growth, and that co-additized oil has thinner final tribofilms than those formed in PAO + ZrO_2. The latter observation matches that of Elinski et al. on the identical system [8]. Finally, we also observe that traction generally increases in magnitude as the tribofilms develop, but defer discussion of this phenomenon to Sect. 3.3.

A surprising trend in these data is that tribofilm growth is non-monotonic—interruptions of tribofilm growth occur for nearly every set of conditions (Fig. 1, gray circled regions). This effect was not observed in the nanoscale AFM results of Khare et al. [20]. Non-monotonic tribofilm growth is seen in the MTM studies of the same ZrO_2 NCs in Elinski et al. [8] and Thrush et al. [22, 30] but these works did not examine the causes of this effect. Khare et al.'s [20] AFM study of nanoscale ZrO_2 tribofilm growth reported that tribofilm removal processes do occur, but the removal was limited to the upper few nanometers of tribofilm once it reached its maximum height, and did not lead to substantial changes in tribofilm height during the growth phase, unlike the transient periods of Fig. 1. Meanwhile, studies on other metal oxide nanoparticles, such as ZnO [9, 31] or CuO [17], tend to focus on steady-state AW performance without interrogating tribofilm growth kinetics. In contrast to these prior studies, we can observe non-monotonic tribofilm growth clearly when it occurs, because we obtained SLIM images

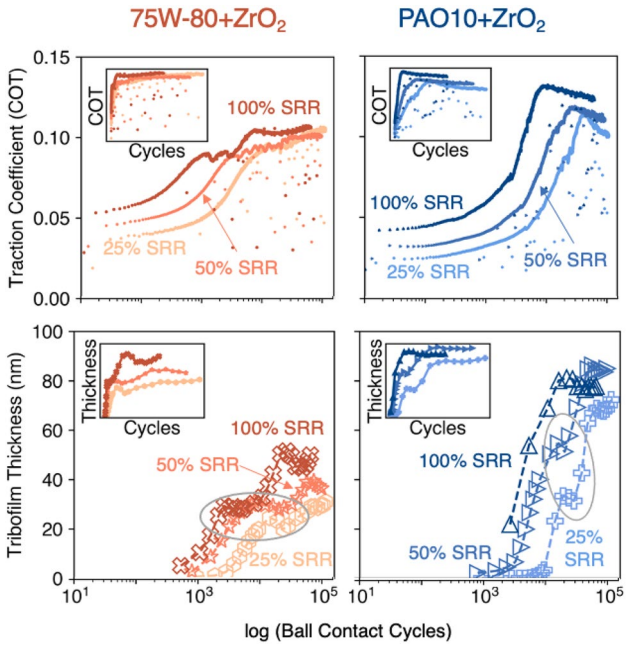

Fig. 1 Traction and ZrO_2 tribofilm evolution data as a function of contact cycles in mixed rolling/sliding experiments (conditions specified in Tables 1 and 2). Left: experiments in 75W-80; Right: experiments in PAO10; Top: traction coefficient; Bottom: tribofilm thickness. The insets provide linear plots of the same data. For every condition save PAO10 + ZrO_2 at 100% SRR, the tribofilm growth regime is non-monotonic (highlighted with gray ovals)

at a relatively high rate of one image per minute for the first 10 min of each MTM test (except for PAO10 at 100% SRR, whose first SLIM image occurs at 10 min). The evidence of non-monotonic tribofilm growth is a clue to elucidate the mechanisms by which NC-based tribofilms form and stabilize.

3.2 Removal Competes with Tribosintering

Figure 2 demonstrates that the non-monotonic tribofilm growth observed in Fig. 1 is the cumulative effect of tribofilm *removal* from the ball specimen outpacing growth. (Supporting Information includes annotated movies for a more comprehensive look at these data.) Because SLIM is an interferometric optical technique, we can assume that this change in tribofilm thickness is real, rather than an artifact due to a plastically deformed substrate beneath the tribofilm (as observed in the MPR experiments of [25]). It is also unlikely that the non-monotonic events are merely artifacts of refractive index changes in the tribofilm as it densifies [32], particularly since successive ZrO_2 removal and regrowth events were observed in the SLIM images for all SRRs and blends under consideration. This removal does not occur as a single global delamination or failure of the tribofilm, but as the local thinning of patches or azimuthal

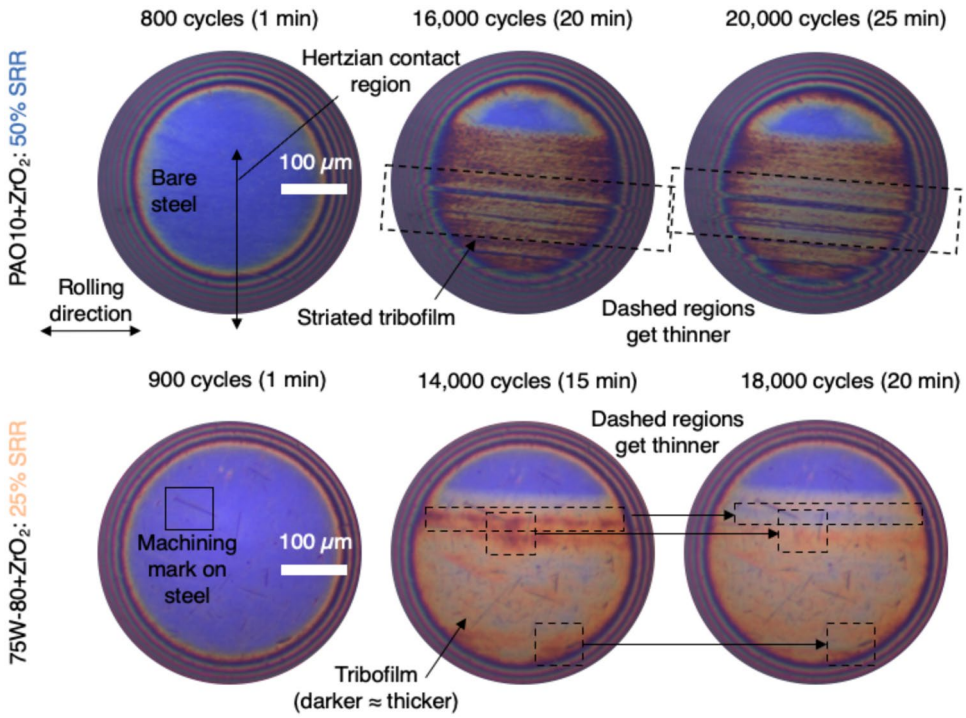

Fig. 2 Annotated, cropped, representative SLIM images demonstrating the tribofilm removal phase. The left-most images show the steel MTM ball (blue in appearance) with relatively few contact cycles and no visible tribofilm. As the ball undergoes contact cycles in mixed rolling/sliding, a tribofilm builds up and is visible in SLIM as patches and striations—the darker in shade, the thicker the tribofilm. The rightmost images show that, with additional cycles, regions of the tribofilm get thinner, and that this thinning can occur via the removal of local patches or striations in the running direction. Removal is observed in both PAO10 blends (top) and 75W-80 blends (bottom), leading to a transient phase involving an overall net decrease in mean tribofilm thickness, as seen in Fig. 1

bands of tribofilm throughout the Hertzian ball-disc contact. When these events were averaged to obtain Fig. 1, the cumulative effect of these events led to non-monotonicity. In other words, tribofilm removal is not a single event, but occurs constantly in competition with tribosintering-driven growth; the non-monotonic periods of Fig. 1 are simply the moments when removal outpaces tribosintering on average (PAO10 + ZrO_2 at 100% SRR was the one case where local removal never outweighed growth in this way). When the two processes occur at equal rates, we see a plateau of growth; at steady state, Khare et al. dubbed this saturation.

3.3 Test Conditions Change Removal Process

The competition between tribofilm removal and tribosintering dictates tribofilm growth kinetics and steady-state tribofilm thickness. This is evident in the differences between the PAO10 and 75W-80 experiments of Fig. 1—co-additives disrupt the balance between removal and growth, leading to different kinetics (see Sect. 3.5), and thinner steady-state tribofilm thicknesses by a factor of almost 2. However, to understand the importance of the removal process for tribofilm properties and performance, we utilize an ex situ study of tribofilm morphology.

Examination of the end-of-test morphologies of the MTM ball and disc specimens show that the tribofilms formed in 75W-80 + ZrO_2 have uniformly smoother surfaces than those formed without co-additives at the same SRR (ball specimens shown in Fig. 3; disc specimens are similar and displayed in SI1, and bearing areas of these films are examined in SI2). There is also a modest but clear trend for both blends that as the SRR increases, so does the composite roughness of the interface $R_q = \sqrt{R_{q,ball}^2 + R_{q,disk}^2}$. We examined the bearing area of the tribofilms to confirm this interpretation (Supporting Information). Taken together, these results show that co-additives cooperate with ZrO_2 to form a smoother tribofilm that bears contact more evenly than tribofilms formed in PAO10 + ZrO_2.

These changes in tribofilm morphology have significant benefits for the ultimate performance of the tribofilms. We can predict one such benefit using the definition of the non-dimensional EHD film thickness λ, the ratio between EHD fluid film thickness and the composite RMS roughness of the interface R_q. Smoother interfaces imply a larger λ ratio, with more surface separation and a lower-traction coefficient, all else equal. Therefore, the change in the interfacial roughness due to co-additives or SRR, without changing the

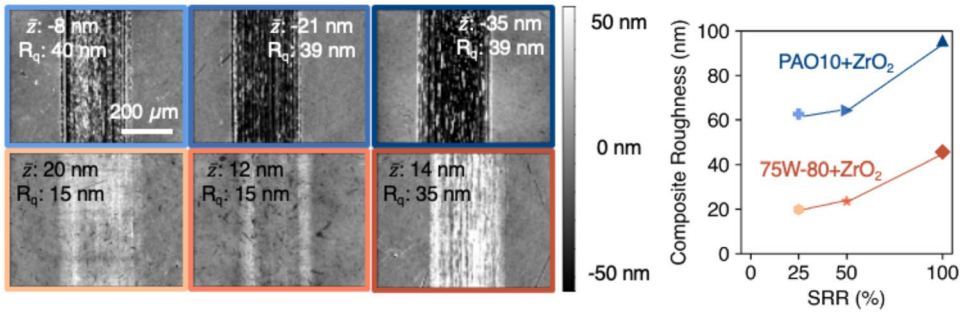

Fig. 3 Left: End-of-test morphologies for white light interferometry (WLI) of MTM ball specimens on which tribofilms were formed in 2 h of rolling-sliding contact (top: PAO10; bottom: 75W-80). The RMS roughness $R_{q,ball}$ and mean tribofilm heights $\bar{z}$ with respect to the substrate are indicated on each plot. Right: End-of-test composite RMS roughness R_q for the MTM ball and disc tribofilm surfaces, with connecting lines to guide the eye

EHL response of the lubricant rheology, should also lead to changes in traction in the boundary regime. For these experiments, the initial λ, estimated using the Hamrock–Dowson equation, is 2.00 ± 0.03 for both PAO10 and 75W-80, putting the contact in the mixed lubrication regime. However, λ decreases as rough tribofilms form in the interface, reaching the boundary lubrication regime, where the contact is asperity-mediated, at about 10 nm of composite roughness. Note that the initial composite areal roughness of the bare steel surfaces is 5–10 nm. We next make use of this insight with a novel analysis method to obtain high time-resolution measurements of the character of the tribological interface.

3.4 Traction Estimates Tribofilm Growth with High Time Resolution

SLIM is not an ideal technique to measure tribofilm growth with high time resolution, as it requires pausing the test for each SLIM image to be acquired, thus slowing down the experiment and creating a practical limit to image rate. However, traction data, collected in situ in the MTM, are sampled by default at 1 Hz. Traction is a force transmitted across an interface [3], and because our experiments progress into the boundary regime as rough tribofilms grow in the interface, we expect that a change in the interface—like wear or tribofilm growth—would lead to a change in the traction coefficient. Figure 4 plots SLIM thickness data and SLIM RMS roughness data against the MTM traction data for both PAO10 + ZrO_2 and 75W-80 + ZrO_2, validating the expectation of a nearly linear thickness-traction correlation over a substantial range of thicknesses. Notably, this does not apply below SLIM thickness values of ~ 5–10 nm, partly because the SLIM measurement uncertainty is of a similar magnitude, and partly because the initial λ ratio for these tests is above 1. However, once the growth of a rough tribofilm instantiates, a quasi-linear correlation holds within the range of 10–50 nm of tribofilm growth, our region of

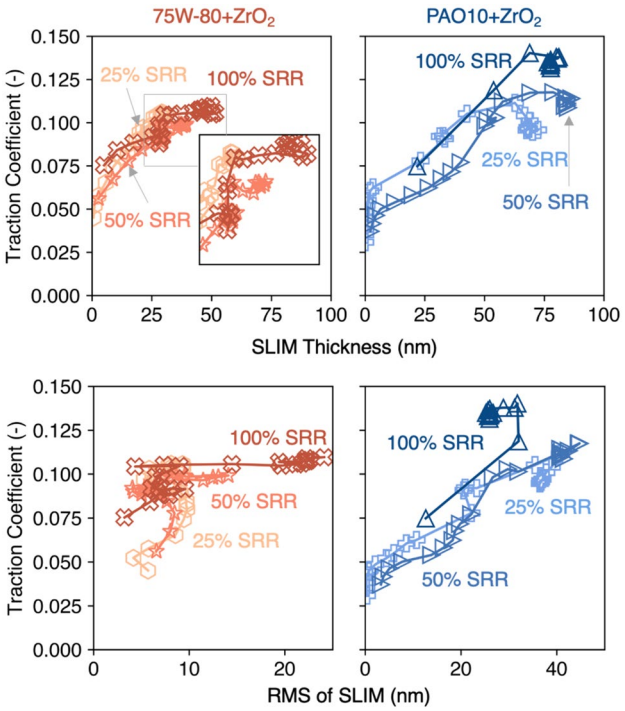

Fig. 4 Top: An approximately linear correlation between traction and SLIM signals under boundary contact conditions for all but the lowest (below ~ 10 nm) and highest (above ~ 50 nm) tribofilm thicknesses. This holds for all SRRs and blends under consideration (left: 75W-80, right: PAO10). The inset on 75W-80 magnifies the region outlined in gray. Bottom: The RMS of the SLIM signal is well correlated with traction in the case of PAO10, but not for 75W-80. In all graphs, the connecting lines represent the vector of time (generally left-to-right) during an MTM test

interest for growth kinetics. Below 10 nm in thickness, the uncertainty of the SLIM instrument makes quantification unreliable; above approximately 50 nm in thickness, most of these ZrO_2 tribofilms have plateaued in height. Therefore, if we remain in boundary contact conditions, and if the

tribofilm is in a formation regime rather than induction or steady state, then we can draw inferences about the interface using the 1 Hz traction signal to qualitatively fill gaps in the 1/60th Hz SLIM signal.

The correlation between RMS roughness of SLIM and traction coefficient is less clear. PAO10 + ZrO_2 displays a clear correlation regardless of SRR, but 75W-80 + ZrO_2 does not. The 100% SRR case, for example, has a nearly 5 × spread in RMS values without significant change to the traction coefficient. Roughness does affect the traction coefficient, but it is not the only process to do so.

This technique enables new experimental approaches to take advantage of the MTM-SLIM system. It can be used to save time over long MTM tests by acquiring less SLIM data without loss of nuance, or even to augment ex situ tribofilm measurements with traction data if SLIM is unavailable, or if tribofilm formation only occurs on the disc which SLIM does not image (this could happen, for instance, with dissimilar ball and disc materials). Indeed, for these data, we supplement the 6 MTM-SLIM experiments shown in Fig. 1 with an additional 18 traction-only MTM tests for the sake of replication (viewable in SI3). The traction trends shown throughout the remainder of this paper are the averages of 4 experiments (n = 4) per combination of SRR and blend. However, we did not attempt (nor do we recommend) the use of curve-fits to *predict* SLIM thickness values using a recorded traction signal. Rather, we use traction as corroboration and context for the SLIM thickness data.

3.5 Co-additives Alter Tribological Interface During Growth

For all tribofilm-forming blends in this study, observable tribofilm growth begins near 10^3 contact cycles (Fig. 5). After this initial growth period, we observe non-monotonic tribofilm growth via SLIM, indicating that removal processes overtake growth processes (Fig. 2), followed by net growth again, eventually reaching a steady-state for the last portion of each test. As a first-order, lower-bound approximation, RMS values from the SLIM data add context to the end-of-test morphologies shown in Fig. 3 by providing cycle-resolved information during tribofilm growth (namely, that RMS tends to increase with the mean SLIM value). Apart from this commonality, the behavior of traction, thickness, and roughness varies significantly as a function of SRR and co-additive.

For example, 75W-80 + ZrO_2 at 25% and 50% SRR have very uniform RMS SLIM values throughout the entire test, unlike the corresponding PAO10 tests. As well, all three co-additized tribofilms are, by the end of experiment, 1.6x–2.3× thinner and 1.1x –4.8× smoother than their PAO10 analogs. One reason for these differences is already suggested by Figs. 1–3: tribofilm removal processes. The

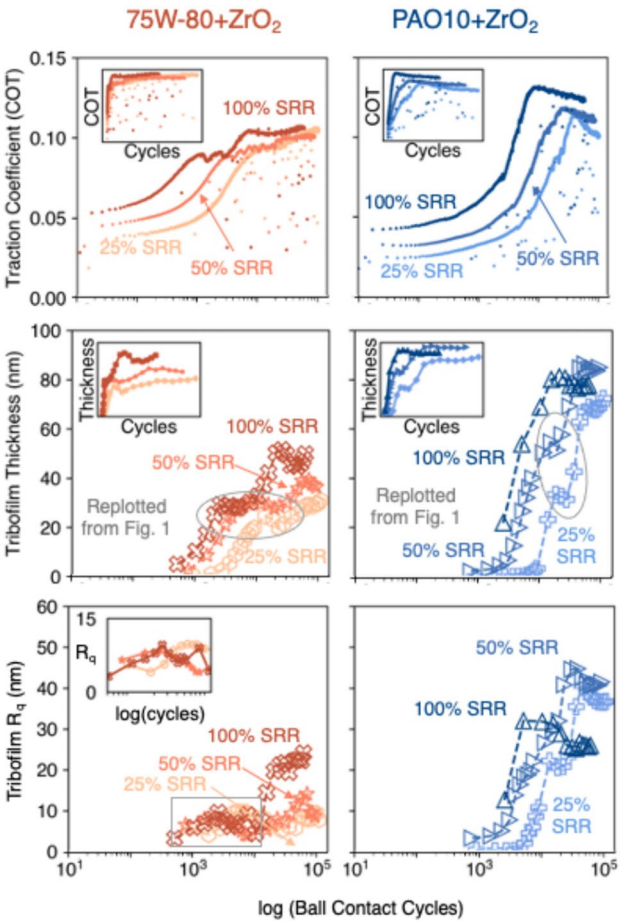

Fig. 5 Tribofilm interfacial traction data (top), SLIM tribofilm thickness (middle row), and the RMS of the SLIM thickness (bottom) *vs.* logarithmic ball cycles for ZrO_2 tribofilms grown in mixed rolling/sliding experiments. The right set of plots describes tribofilms formed from ZrO_2 in PAO10, while the left set is for ZrO_2 in the co-additized 75W-80 oil. The insets for the traction and SLIM thickness data are plotted on a linear scale for ball cycles for comparison (with the same vertical range as each full plot). The inset for the 75W-80 RMS SLIM thickness magnifies the outlined region for clarity

co-additives present in 75W-80 + ZrO_2 apparently make tribofilm removal more favorable than in PAO10 blends, hence a thinner final tribofilm in Figs. 1, 5. However, that same removal also polishes the interfaces of 75W-80-based tests to be smoother at end of test (Fig. 3) and during the latter stages of growth (Fig. 5) compared to the PAO10-based formulation at each SRR. A more polished tribofilm bears contact more evenly (SI 2) and shifts the EHD lubrication regime toward mixed contact, giving a lower-traction signal during the majority of the MTM experiments (Fig. 5).

Note, however, that 75W-80 + ZrO_2 formulations have slightly *higher* traction (1.4x–1.6x) during the initial 10^3 cycles of contact than the PAO10 + ZrO_2 formulations, before the tribofilms are fully formed. It may be that the S- and P-based co-additives are reacting with surface

steel to prevent early scuffing in the interface [8], and/or that the ZrO_2 tribofilm initially grows more quickly due to chemical cooperation with the co-additives (discussed further in Sect. 3.7). Either way, after the removal rates of 75W-80 + ZrO_2 tribofilms begin to temporarily equal and/or outstrip tribofilm growth rates, as demonstrated by SLIM, traction grows less quickly, suggesting that removal and polishing does indeed lead to more favorable traction conditions.

This further supports the hypothesis that, for the boundary contact regime, tribofilm removal acts to polish the tribofilm and increases the λ ratio, decreasing traction. This polishing, the removal of local outliers seen in Fig. 2, appears to be more significant in the presence of co-additives, which explains why the traction coefficients for the 75W-80-based blends are generally lower than that of the PAO10-based blends after the non-monotonic film thickness events (i.e., after the moments when removal outstrips growth). We hypothesize that, if the S- and P-based co-additives in 75W-80 are incorporated into ZrO_2 tribofilm, they promote faster-growing but less removal-resistant tribofilms, leading to a smoother and lower-traction interface as the tribofilm reaches steady state.

3.6 Co-additives Are Incorporated into Tribofilm

To further test the hypothesis that co-additives contribute to the smoother and lower-traction tribofilms at the end of test, we used ToF-SIMS to measure the chemical constituents of the steady-state tribofilm formed on the steel MTM disc in 75W-80 + 1wt%ZrO_2 at 50% SRR (a replicate of the specimen shown in Figs. 1, 2, 3). As ToF-SIMS does not give absolute concentrations (*i.e.*, a similar ion count per extraction does not imply two elements have similar concentrations in the sample), this technique is only used here to confirm elemental abundance—relative to that element—as a function of depth.

Figure 6 confirms that the steady-state tribofilm is comprised of Zr and O species. The 52,100 steel substrate means Fe is also present; because the ToF-SIMS measurement did not etch all the way to the substrate, we cannot be certain whether Fe is a trace signal or is intermixed with the ZrO_2. However, TEM lamella analyzed for similar ZrO_2 tribofilms formed in MPR tests show a sharp Fe-ZrO_2 interface [25], and ToF-SIMS results from Elinski et al. (albeit a different ToF-SIMS instrument, with different primary beam and other settings) show far more Fe in the substrate than in the tribofilm region [8].

Additionally, several P-containing species are seen in the negative polarity spectrum(S-containing species are also possible, but the S peak is convoluted with O_2). The 75W-80 oil is formulated with phosphorus- and sulfur-based (P/S) EP additives, resulting in 0.1–0.17 wt% P and 2.0–2.7 wt%

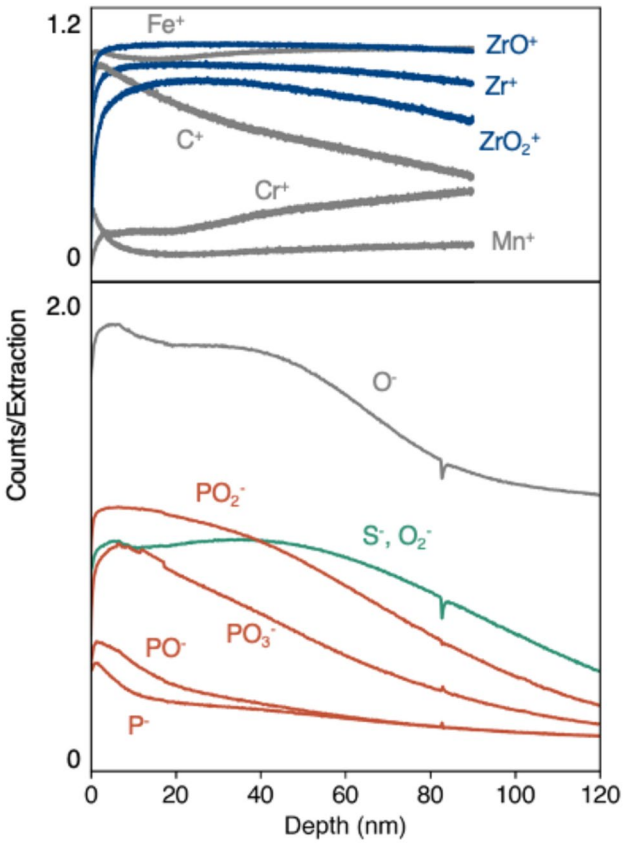

Fig. 6 Chemical depth profiles measured by ToF-SIMS of the tribofilm formed on the steel MTM disc in 75W-80 + 1wt%ZrO_2 at 50% SRR. Bottom: negative polarity profiles; top: positive polarity profiles. P- and S-containing species (red and green profiles, respectively) coincide with Zr species (blue profiles) for tens of nm into the surface of the tribofilm, evidence of integration of co-additives into the tribofilm. Species originating as components of the steel substrate are shown in gray

S in the finished product [33], but the specific molecular details are proprietary. Though the 52,100 steel substrate has C, Cr, and Mn inclusions [34], as well as a native oxide surface layer, P and S are minimal in the steel (< 0.025 wt.% [34]) and in the ZrO_2 nanocrystals. Therefore, P- and S-containing species present in the ZrO_2 tribofilm for tens of nm of depth (Fig. 6) can be attributed to the incorporation of P- and S-based EP co-additives into the tribofilm at non-negligible levels, potentially influencing the growth and removal processes and the tribological properties of the tribofilm. This supports the hypotheses posed above that incorporated co-additives influence the balance between tribosintering and tribofilm removal processes, in most cases leading to a smoother and thinner film, and a lower-traction interface at steady state than for ZrO_2 alone (Fig. 5). The co-additives lead to smoother ZrO_2 interfaces once steady state is reached (Fig. 3), but the physico-chemical mechanisms by which these processes occur remain to be understood. Efforts to

understand this using the quantum chemical calculations of ab initio density functional theory (DFT) are in progress on models representative of the 75W-80/ZrO_2/ligand system and will be the subject of a future publication.

3.7 Growth Kinetics and Formation Mechanisms

To compare the growth kinetics explicitly, we isolated the growth stages of each SLIM and traction signal (Fig. 7) and estimated their growth rates (SI 3 and SI 4). The earliest work on these ZrO_2 nanocrystals proposed a 3-phase tribosintering mechanism for film formation, supported by later studies on the same NC system [8, 20, 23]: an induction period of no observable growth, a nearly linear growth phase, and a steady-state phase. As discussed above, in most of our MTM experiments, the growth phase exhibited transient reversals of tribofilm growth, attributed to removal processes overtaking growth processes. For those cases, we calculated two linear stages of growth, before (filled data markers and colorful guidelines) and after (hollow data markers and gray guidelines) the transient.

The increased SRR negligibly changes the initial growth rate from SLIM for PAO10 + ZrO_2, but significantly increases that of 75W-80 + ZrO_2 (Fig. 7, left). The traction data exhibit the same trend (Fig. 7, right), consistent with our contention in Sect. 3.3 that traction may be taken to be a higher time-resolution proxy for tribofilm growth for the linear growth stages of the experiment. The latter also allows us to leverage our large experimental dataset for the n = 4 trials for each set of conditions. Moreover, the increased initial growth rate with increased SRR for 75W-80 + ZrO_2 provides new and strong support for the claim by Elinski et al. [8] that the S- and P-based co-additives cooperate with ZrO_2 to promote faster tribofilm growth that largely prevents the moderate amount of early-stage wear of the substrate that occurs with PAO10 + ZrO_2.

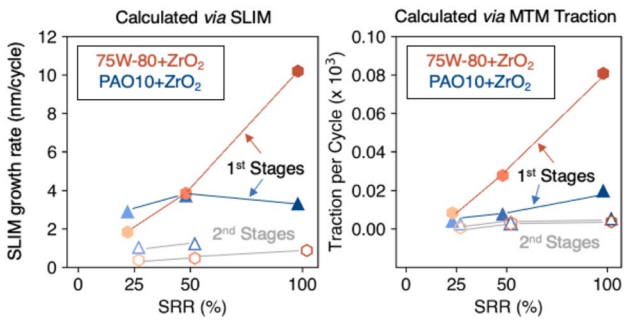

Fig. 7 Average growth rates as a function of sliding speed and lubricant co-additives, derived from SLIM (left, number of trials n = 1) and traction (right, n = 4). The slopes are obtained from linear fits before and after any net-negative removal events (method in SI3); the latter linear stage is plotted with hollow data points and gray lines to guide the eye and offset right to illustrate the temporal ordering. Blue lines guide the eye for the initial rates of PAO10 blends, and orange lines do the same for those of 75W-80. Increasing the SRR has a stronger positive effect on the growth rates of ZrO_2 tribofilms in 75W-80

When tribosintering again outpaced tribofilm removal after the transient period (*i.e.*, during the second linear stage), the growth rates were consistently smaller than during the first linear stage in all cases. Especially striking was that the strongly SRR-dependent growth rates seen for 75W-80 + ZrO_2 prior to the transient period no longer occur; their kinetics resemble those of additive-free PAO10 + ZrO_2. Co-additives thus boost tribosintering rates of ZrO_2 only during the first linear stage. While we are unable to formulate a mechanism to explain this presently, we will attempt to use the aforementioned DFT simulations to determine whether and how S and P chemistries alter the chemical affinity of ZrO_2 surfaces in ways that would alter growth and removal processes including sintering, abrasion, and adhesive transfer.

4 Conclusions

Metal oxide nanocrystal additives quickly form robust antiwear films under a variety of conditions that normally lead to scuffing and micropitting [8, 20, 22–25], including in fully formulated commercial gear oils with lower viscosities intended to increase energy efficiency [26]. This work unlocks new insights into metal oxide nanocrystal tribofilm formation by pairing in situ tribofilm thickness measurements via SLIM with analysis of high-resolution traction data in MTM experiments.

We attributed the interrupted, two-stage growth of ZrO_2 tribofilms to transient tribofilm removal events observed with SLIM. Traction coefficients and thickness values were correlated during most of the tribofilm growth phase, including when tribofilm removal events temporarily outpaced growth. This correlation assumes boundary contact, tribofilms thicker than the SLIM's measurement error (5–10 nm), and tribofilms not yet saturated in thickness. Thus, high time-resolution traction measurements can, with caution, be used as proxies to track tribofilm growth kinetics to supplement SLIM measurements and/or provide replication of trends without the need to perform additional SLIM measurements, thus increasing experimental throughput.

The addition of industry-standard S- and P-based AW and EP co-additives to a PAO-based, ZrO_2-containing lubricant:

- increases the initial growth rate of tribofilms. We propose that this contributes to the superior anti-scuffing performance these blends exhibit compared to those with ZrO_2 alone;

- enhances tribofilm polishing to generate overall thinner tribofilms but with smoother tribofilm surfaces, and thus more favorable lubrication conditions; and
- does not affect the second-stage tribofilm growth rate (*i.e.*, after tribofilm removal outpaces tribofilm growth).

As S and P are incorporated into the tribofilms, all of the above effects may be driven by chemical mechanisms that will be the subject of future investigation.

In summary, consistent with earlier work, we demonstrate in further depth here that S- and P-based co-additives provide substantial benefits for ZrO_2 tribofilm performance [8]. This work offers a more precise look at the qualities and features of tribofilm performance which are improved by the cooperative behavior of co-additives and ZrO_2.

Future work will explore the removal mechanisms of the tribofilm. Several mechanisms are possible: adhesive transfer of ZrO_2 to the MTM disc specimen (as the disc's tribofilm is not measured in SLIM), abrasive wear of the tribofilm, plastic flow, and/or erosive wear (which is unlikely because of the boundary contact in these conditions). MTM, AFM, and nanoindentation techniques are being used to explore these, along with DFT calculations. Whatever the mechanism, this connection between co-additives and tribofilm removal is perhaps most important when it comes to growth kinetics, so that ZrO_2 tribofilms can form rapidly and thus prevent failure of contacting parts.

Supplementary Information The online version contains supplementary material available at https://doi.org/10.1007/s11249-024-01905-w.

Acknowledgements We gratefully acknowledge support from the U.S. Army Combat Capabilities Development Command Ground Vehicle Systems Center (CCDC GVSC) under Small Business Technology Transfer (STTR) Phase II Award Number DE-SC-0009222, and from DOE EERE Advanced Manufacturing Office under Award DE-EE0010211. This work was carried out in part at the Singh Center for Nanotechnology, which is supported by the NSF National Nanotechnology Coordinated Infrastructure Program under grant NNCI-2025608. M.B.E. acknowledges support from the University of Pennsylvania Provost Postdoctoral Fellowship program. P.L. acknowledges support from the National Defense Science and Engineering Graduate Fellowship Program.

Author Contributions All authors contributed to the study conception and design. Nanocrystals and formulations were prepared by L.Z. and R.J.W. Data collection and analysis were performed by P.L., M.B.E., D.D., P.N., and J.G. The manuscript was drafted by P.L. with significant input from J.G. and D.D., and overseen and edited by R.W.C. All authors read and approved the final manuscript.

Funding We gratefully acknowledge support from the U.S. Army Combat Capabilities Development Command Ground Vehicle Systems Center (CCDC GVSC) under Small Business Technology Transfer (STTR) Phase II Award Number DE-SC-0009222, and from DOE EERE Advanced Manufacturing Office under Award DE-EE0010211. This work was carried out in part at the Singh Center for Nanotechnology, which is supported by the NSF National Nanotechnology Coordinated Infrastructure Program under grant NNCI-2025608.*M.B. Elinski acknowledges support from the University of Pennsylvania Provost Postdoctoral Fellowship program. P. LaMascus acknowledges support from the National Defense Science and Engineering Graduate Fellowship Program.*

Data Availability Data unavailable.

Declarations

Competing Interests L.Z., A.J., and R.J.W. are affiliated with the commercial vendor for the ZrO2 nanocrystals (Pixelligent Technologies, LLC). L.Z. and R. J.W. are employees of Pixelligent and have equity in the company. A.J. is a consultant to Pixelligent. No other coauthors declare competing financial interest.

References

1. Mate, C.M., Carpick, R.W.: Tribology on the small scale: a modern textbook on friction, lubrication and wear. In: Oxford Graduate Texts, 2nd edn. Oxford University Press, Oxford (2019)
2. Holmberg, K., Erdemir, A.: The impact of tribology on energy use and CO_2 emission globally and in combustion engine and electric cars. Tribol. Int. **135**, 389–396 (2019). https://doi.org/10.1016/j.triboint.2019.03.024
3. Stachowiak, G.W., Batchelor, A.W.: Engineering tribology, 4th edn. Elsevier Butterworth-Heinemann, Amsterdam (2014)
4. Spikes, H.: The history and mechanisms of ZDDP. Tribol. Lett. **17**(3), 469–489 (2004). https://doi.org/10.1023/B:TRIL.0000044495.26882.b5
5. Gosvami, N.N., Bares, J.A., Mangolini, F., Konicek, A.R., Yablon, D.G., Carpick, R.W.: Mechanisms of antiwear tribofilm growth revealed in situ by single-asperity sliding contacts. Science **348**(6230), 102–106 (2015). https://doi.org/10.1126/science.1258788
6. Fang, L., Korres, S., Lamberti, W.A., Webster, M.N., Carpick, R.W.: What stress components drive mechanochemistry? A study of ZDDP tribofilm formation. Faraday Discuss. **241**, 394–412 (2023). https://doi.org/10.1039/D2FD00123C
7. Ran, X., Yu, X., Zou, Q.: Effect of particle concentration on tribological properties of ZnO nanofluids. Tribol. Trans. **60**(1), 154–158 (2017). https://doi.org/10.1080/10402004.2016.1154233
8. Elinski, M.B., LaMascus, P., Zheng, L., Jackson, A., Wiacek, R.J., Carpick, R.W.: Cooperativity between zirconium dioxide nanoparticles and extreme pressure additives in forming protective tribofilms: toward enabling low viscosity lubricants. Tribol. Lett. **68**(4), 107 (2020). https://doi.org/10.1007/s11249-020-01346-1
9. Mariño, F., et al.: ZnO nanoparticles coated with oleic acid as additives for a polyalphaolefin lubricant. J. Mol. Liq. **348**, 118401 (2022). https://doi.org/10.1016/j.molliq.2021.118401

10. Kato, H., Komai, K.: Tribofilm formation and mild wear by tribo-sintering of nanometer-sized oxide particles on rubbing steel surfaces. Wear **262**(1–2), 36–41 (2007). https://doi.org/10.1016/j.wear.2006.03.046
11. Rudnick, L.: Lubricant additives: chemistry and applications, 2nd ed. In: Chemical Industries, vol. 124. CRC Press, New York (2009)
12. UNFCCC: The Paris Agreement. United Nations, Nov. 2015. http://unfccc.int/files/essential_background/convention/application/pdf/english_paris_agreement.pdf
13. EPA announces the 'Clean Trucks Plan:' Office of transportation and air quality, Aug. 2021. https://nepis.epa.gov/Exe/ZyPDF.cgi?Dockey=P1012ON0.pdf. Accessed 09 Nov 2022
14. Infineum: Service fill oils for gasoline, light-duty diesel and heavy-duty diesel engines. https://www.infineum.com/media/w5kpot0y/api-engine-oil-classifications-brochure2.pdf. Accessed 26 Jan 2023
15. Adachi, K., Kato, K.: Formation of smooth wear surfaces on alumina ceramics by embedding and tribo-sintering of fine wear particles. Wear **245**(1–2), 84–91 (2000). https://doi.org/10.1016/S0043-1648(00)00468-3
16. Hernández Battez, A., et al.: Wear prevention behaviour of nanoparticle suspension under extreme pressure conditions. Wear **263**(7–12), 1568–1574 (2007). https://doi.org/10.1016/j.wear.2007.01.093
17. Hernández Battez, A., et al.: CuO, ZrO2 and ZnO nanoparticles as antiwear additive in oil lubricants. Wear **265**(3–4), 422–428 (2008). https://doi.org/10.1016/j.wear.2007.11.013
18. Dai, W., Kheireddin, B., Gao, H., Liang, H.: Roles of nanoparticles in oil lubrication. Tribol. Int. **102**, 88–98 (2016). https://doi.org/10.1016/j.triboint.2016.05.020
19. Liu, G., Li, X., Qin, B., Xing, D., Guo, Y., Fan, R.: Investigation of the mending effect and mechanism of copper nano-particles on a tribologically stressed surface. Tribol. Lett. **17**(4), 961–966 (2004). https://doi.org/10.1007/s11249-004-8109-6
20. Khare, H.S., et al.: Nanoscale generation of robust solid films from liquid-dispersed nanoparticles via in situ atomic force microscopy: growth kinetics and nanomechanical properties. ACS Appl. Mater. Interfaces **10**(46), 40335–40347 (2018). https://doi.org/10.1021/acsami.8b16680
21. Zhang, J., Spikes, H.: On the mechanism of ZDDP antiwear film formation. Tribol. Lett. **63**(2), 24 (2016). https://doi.org/10.1007/s11249-016-0706-7
22. Thrush, S.J., et al.: Stability, thermal conductivity, viscosity, and tribological characterization of zirconia nanofluids as a function of nanoparticle concentration. Tribol. Trans. **63**(1), 68–76 (2020). https://doi.org/10.1080/10402004.2019.1660017
23. Thrush, S.J., et al.: Study of pressure dependence on sinterable zirconia nanoparticle tribofilm growth. Tribol. Int. **154**, 106683 (2021). https://doi.org/10.1016/j.triboint.2020.106683
24. Thrush, S.J., et al.: Growth and morphology of thermally assisted sinterable zirconia nanoparticle tribofilm. Tribol. Int. **175**, 107820 (2022). https://doi.org/10.1016/j.triboint.2022.107820
25. Lahouij, I., et al.: Inhibition of micro-pitting by tribofilm-forming ZrO_2 nanocrystal lubricant additives: a micro-pitting rig and transmission electron microscope study. Tribol. Lett. **70**(1), 13 (2022). https://doi.org/10.1007/s11249-021-01555-2
26. Demas, N.G., Gould, B.J., Greco, A.C., Lorenzo-Martin, C., Erck, R.A., Ajayi, O.O.: Scuffing performance of low viscosity gear oil containing ZrO2 nanocrystals. Proc. STLE ASME Int. Jt. Tribol. Conf. **1**, 1 (2019)
27. Elinski, M.B., LaMascus, P., Zheng, L., Jackson, A., Wiacek, R.J., Carpick, R.W.: Correction to: cooperativity between zirconium dioxide nanoparticles and extreme pressure additives in forming protective tribofilms: toward enabling low viscosity lubricants. Tribol. Lett. **69**(4), 140 (2021). https://doi.org/10.1007/s11249-021-01510-1
28. Spikes, H.A., Cann, P.M.: The development and application of the spacer layer imaging method for measuring lubricant film thickness. Proc. Inst. Mech. Eng. Part J **215**(3), 261–277 (2001). https://doi.org/10.1243/1350650011543529
29. Benedet, J., Green, J.H., Lamb, G.D., Spikes, H.A.: Spurious mild wear measurement using white light interference microscopy in the presence of antiwear films. Tribol. Trans. **52**(6), 841–846 (2009). https://doi.org/10.1080/10402000903180696
30. Thrush, S.J., et al.: Wear mechanisms of a sintered tribofilm in boundary lubrication regime. Wear **482–483**, 203932 (2021). https://doi.org/10.1016/j.wear.2021.203932
31. Gara, L., Zou, Q.: Friction and wear characteristics of oil-based ZnO nanofluids. Tribol. Trans. **56**(2), 236–244 (2013). https://doi.org/10.1080/10402004.2012.740148
32. Jerman, M., Qiao, Z., Mergel, D.: Refractive index of thin films of SiO_2, ZrO_2, and HfO_2 as a function of the films' mass density. Appl. Opt. **44**(15), 3006 (2005). https://doi.org/10.1364/AO.44.003006
33. Blumenfeld, M.: Personal Communication
34. AISI E 52100 Steel (100Cr6, SUJ2,UNS G52986). Matweb.com. https://www.matweb.com/search/DataSheet.aspx?MatGUID=d0b0a51bff894778a97f5b72e7317d85. Accessed Apr 07, 2024